J|A|C|S ARTICLES

Published on Web 08/25/2010

Mechanism and Activity of Photocatalytic Oxygen Evolution on Titania Anatase in Aqueous Surroundings

Ye-Fei Li,[†] Zhi-Pan Liu,*[,†] LuLu Liu,[‡] and Weiguo Gao[‡]

Shanghai Key Laboratory of Molecular Catalysis and Innovative Materials, Department of Chemistry, Key Laboratory for Computational Physical Sciences, Ministry of Education, Fudan University, Shanghai 200433, China, and School of Mathematical Sciences, Fudan University, Shanghai 200433, China

Received June 18, 2010; E-mail: zpliu@fudan.edu.cn

Abstract: Due to its high overpotential and low efficiency, the conversion of water to O_2 using solar energy remains a bottleneck for photocatalytic water splitting. Here the microscopic mechanisms of the oxygen evolution reaction (OER) on differently structured anatase surfaces in aqueous surroundings, namely, (101), (001), and (102), are determined and compared systematically by combining first-principles density functional theory calculations and a parallel periodic continuum solvation model. We show that OER involves the sequential removal of protons from surface oxidative species, forming surface peroxo and superoxo intermediates. The initiating step, the first proton removal, dictates the high overpotential. Only at an overpotential of 0.7 V (1.93 V vs SHE) does this rate-controlling step become surmountable at room temperature: the free energy change of the step is 0.69, 0.63, and 0.61 eV for (101), (102), and (001) surfaces, respectively. We therefore conclude that (i) OER is not sensitive to the local surface structure of anatase and (ii) visible light ($<\sim$590 nm) is, in principle, capable of driving the photocatatlytic OER on anatase kinetically. By co-doping high-valent elements into the anatase subsurface, we demonstrate that the high overpotential of the OER can be significantly reduced, with extra occupied levels above the valence band.

1. Introduction

Photocatalytic water splitting has attracted enormous attention in recent decades since the seminal work of Fujishima and Honda.[1] The reaction is regarded as a prototype surface photocatalytic reaction which can utilize solar energy. As perhaps the most important material in photocatalysis, TiO_2-based materials can act as both anode for O_2 evolution and cathode for H_2 evolution with dopant-induced modifications of the Fermi level and the band gap. To date, one of the key goals in the field has been to reduce the substantial energy loss caused by the high overpotential of the oxygen evolution reaction (OER) on the anode[2] and especially to improve the activity in the visible light regime.[3] Although many elements have been tested for use as dopants, including nitrogen,[4] sulfur,[5] carbon,[6] niobium,[7] antimony, and chromium,[8] it remains a mystery how to design a better visible-light-driven anode to achieve high OER activity, largely because an atomic-level understanding of the chemical process is not yet established.

The photosplitting of water involves first electron−hole pair generation by light irradiation and subsequent separation under an interface electric field.[9−12] For the OER, the accumulation of cationic holes (h^+) on the surface, namely, surface-trapped holes, is believed to be essential, as they are utilized to reduce the adsorbed water via $H_2O_{ad} + 2h^+ \rightarrow {}^1/_2\,O_2 + 2H^+$. One of the most intriguing questions is that of how O_2 evolves from H_2O on TiO_2, considering that atomic oxygen is known to be very unstable on semiconducting oxides. Wilson[13] first identified the formation of oxidative species on a TiO_2 anode by electrochemical scanning. Using the same technology, Salvador and Gutiérrez[14−17] suggested that Wilson's surface species may be attributed to adsorbed H_2O_2, produced by the coupling of surface OH radicals. Nakamura and Nakato[18] proposed that this reaction is initiated by nucleophilic attack of a H_2O molecule on a surface-trapped hole at a surface lattice O, followed by bond-breaking of H_2O, described by $H_2O + O_{lattice} + h^+ \rightarrow$ [Ti−O$^{\bullet}$ HO−Ti] + $H^+ \rightarrow$ Ti−O−O−Ti + $2H^+ \rightarrow O_2 + 4H^+$. Importantly, they identified the surface peroxo (Ti−O−O−Ti) intermediate by *in situ* IR spectroscopy. Due to uncertainties

[†] Department of Chemistry.
[‡] School of Mathematical Sciences.

(1) Fujishima, A.; Honda, K. *Nature* **1972**, *238*, 37.
(2) Nozik, A. J. *Nature* **1975**, *257*, 383.
(3) Zou, Z.; Ye, J.; Sayama, K.; Arakawa, H. *Nature* **2001**, *414*, 625.
(4) Asahi, R.; Morikawa, T.; Ohwaki, T.; Aoki, K.; Taga, Y. *Science* **2001**, *293*, 269.
(5) Ohno, T.; Mitsui, T.; Matsumura, M. *Chem. Lett.* **2003**, *32*, 364.
(6) Irie, H.; Watanabe, Y.; Hashimoto, K. *Chem. Lett.* **2003**, *32*, 772.
(7) Kikkawaa, H.; O'Reganb, B.; Anderson, M. A. *J. Electroanal. Chem.* **1991**, *309*, 91.
(8) Kato, H.; Kudo, A. *J. Phys. Chem. B* **2002**, *106*, 5029.
(9) Fujishima, A.; Rao, T. N.; Tryk, D. A. *J. Photochem. Photobiol. C* **2000**, *1*, 1.
(10) Grätzel, M. *Nature* **2001**, *414*, 338.
(11) Wrighton, M. S. *Acc. Chem. Res.* **1979**, *12*, 303.
(12) Nozik, A. J.; Memming, R. *J. Phys. Chem.* **1996**, *100*, 13061.
(13) Wilson, R. H. *J. Electrochem. Soc.* **1980**, *127*, 228.
(14) Salvador, P.; Gutiérrez, C. *Chem. Phys. Lett.* **1982**, *86*, 131.
(15) Salvador, P.; Gutiérrez, C. *J. Phys. Chem.* **1984**, *88*, 3696.
(16) Salvador, P.; Gutiérrez, C. *J. Electroanal. Chem.* **1984**, *160*, 117.
(17) Salvador, P.; Gutiérrez, C. *Surf. Sci.* **1983**, *124*, 398.
(18) Nakamura, R.; Nakato, Y. *J. Am. Chem. Soc.* **2004**, *126*, 1290.

10.1021/ja105340b

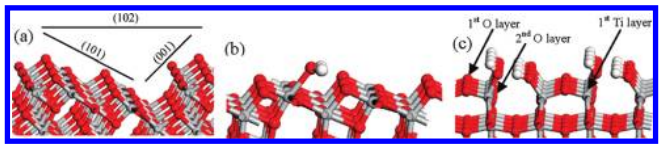

Figure 1. Structures of anatase surfaces: (a) overview of anatase (101), (001), and (102) surfaces; (b) anatase (101) with H_2O adsorption; and(c) anatase (001) with half a monolayer of dissociated H_2O. Ti, gray; O, red; H, white.

in the reaction mechanism, the physical origin of the high overpotential remains unclear. It is of significance to answer whether the overpotential is due to intrinsic difficulties in the kinetics of the multistep reaction process.

Apart from the controversy about the mechanism, it is also intriguing that the photocatalytic reaction appears to be sensitive to the surface morphology in general. The OER has been examined by Ohno et al. on titania particles with mixed anatase and rutile phases (such as commercial P25). They found, interestingly, that rutile is the dominant phase responsible for OER activity.[19] They also found that H_2PtCl_6 prefers to grow into Pt metal on the majority rutile (110) and anatase (101) surface, indicating a higher reduction ability of these surfaces compared to other minority surfaces.[20] The structure dependence of photocatalytic activity was attributed to a number of possible causes, such as the band-bending of surfaces in contact with solution and the local chemical reactivity of the surface sites.

Considering that anatase is the major phase in nanocrystal TiO_2 for particle sizes up to several nanometers, and that small (nanosized) particles can expose much larger surface area,[21] anatase TiO_2 is of particular interest for application in photocatalytic water splitting. In this contribution we have carried out an extensive survey on the possible mechanism of OER on three differently structured anatase surfaces, namely, the majority (101) terrace, the minority (001) terrace, and the monatomic steps as represented by the (102) surface. The (102) step incorporates the (101) and the (001) microfacets, as depicted in Figure 1a, and is one of the elementary steps in anatase.[22] Here we show that the photocatalytic OER needs a high overpotential of 0.7 V on all three surfaces investigated, which is accessible using visible light. Importantly, the activity is not strongly dependent on the local surface structure. The high overpotential of OER originates from the high energy cost of the first proton removal step, which features the formation of surface-adsorbed OH and the oxidized TiO_2 surface. A general strategy for designing a better OER catalyst is then addressed at the atomic level by comparing the activities of rutile, anatase, and doped-anatase systems.

2. Methodology and Calculation Details

2.1. Density Functional Theory Calculations. All density functional theory (DFT) calculations were performed using the SIESTA package[23] with numerical atomic orbital basis sets[24a] and Troullier−Martins norm-conserving pseudopotentials.[24b] The exchange-correlation functional utilized was GGA-PBE,[25] and the double-ξ plus (DZP) polarization basis set was employed. The semicore 3s, 3p states of Ti were included. The cutoff for the real-space grid was set as 150 Ry. The quasi-Newton Broyden method was employed for geometry relaxation until the maximal forces on each relaxed atom were less than 0.1 eV/Å. The convergence of the structural relaxation was checked with the 0.05 eV/Å criterion for the first proton removal step on (101) and (001), and the difference in energy was less than 0.01 eV. The solvation energy due to the long-range electrostatic interaction was computed by a periodic continuum solvation model with a smooth dielectric function (see the next subsection). Transition states (TSs) of the catalytic reaction were searched using the constrained Broyden minimization[26a] and the Broyden dimer method.[26b]

It should be mentioned that the local-density-approximation (LDA) forms of DFT functionals are known to underestimate the band gap of semiconductors. Efforts to improve DFT functionals have been made in recent years, including the semiempirical LDA+U,[27] meta-GGA M06-L,[28a,b] hybrid M06,[28c,d] and PBE0[29] functionals. The band gaps computed at the PBE0 level are 4.05 and 4.50 eV for bulk rutile and anatase TiO_2, respectively[30a] (3.96 and 4.63 eV for rutile (110) and anatase (101), respectively[30b]), which appears to overcorrect the gap (expt ~3.2 eV). In general, the hybrid functionals are highly computationally demanding in calculations with periodic boundary conditions (e.g., ~100 times more expensive) and are rarely utilized for kinetics studies of complex surface reactions. Camellone and Fabris investigated the energy profile of CO oxidation on Au/CeO_2 using PBE and PBE+U and showed that the two approaches provide similar reaction profiles.[31] On the basis of these results, and because a proper inclusion of solvent effects is compulsory in photocatalysis, in this work we adopted the popular PBE functional for the study of OER kinetics.

The anatase surfaces modeled are shown in Figure 1a, and rectangular unit cells are utilized for the surface slabs: (101), 10.398 × 11.448 Å, 144 atoms; (001), 7.632 × 7.632 Å, 96 atoms; and (102), 12.321 × 7.632 Å, 132 atoms. For the three surface slabs, Γ-points and (2×2×1) and (1×2×1) Monkhorst−Pack *k*-point mesh were routinely utilized for energy and structural calculations. The convergence of the *k*-point mesh in calculating the free energy has been checked for key reactions. For example, the free energy of the first proton removal on (001) varies less than 0.1 eV on going from (2×2×1) to (4×4×1) *k*-point mesh. The (101) and (001) surface slabs include 8 Ti layers and 16 O layers (the top Ti and O layers are defined in Figure 1c), with the 4 central Ti layers and 8 central O layers being fixed at bulk-truncated positions. The (102) surface slab contains 10 Ti layers and 20 O layers along the [101] direction, with the 6 central Ti layers and 12 central O layers fixed. The vibrational frequencies of adsorbates were obtained by the numerical finite displacement method, which was essential for zero-point energy (ZPE) correction. These DFT calculation setups have been carefully benchmarked with plane-wave methods. For ex-

(19) Ohno, T.; Sarukawa, K.; Matsumura, M. *J. Phys. Chem. C* **2001**, *105*, 2417.
(20) Ohno, T.; Sarukawa, K.; Matsumura, M. *New J. Chem.* **2002**, *26*, 1167.
(21) Ranade, M. R.; Navrotsky, A.; Zhang, H. Z.; Banfield, J. F.; Elder, S. H.; Zaban, A.; Borse, P. H.; Kulkarni, S. K.; Doran, G. S.; Whitfield, H. J. *Proc. Natl. Acad. Sci. U.S.A.* **2002**, *99*, 6476.
(22) Gong, X. Q.; Selloni, A.; Batzill, M.; Diebold, U. *Nat. Mater.* **2006**, *5*, 665.
(23) Soler, J. M.; Artacho, E.; Gale, J. D.; Garcia, A.; Junquera, J.; Ordejon, P.; Sanchez-Portal, D. *J. Phys.: Condens. Matter* **2002**, *14*, 2745.
(24) (a) Junquera, J.; Paz, O.; Sanchez-Portal, D.; Artacho, E. *Phys. Rev. B* **2001**, *64*, 235111. (b) Troullier, N.; Martins, J. L. *Phys. Rev. B* **1991**, *43*, 1993.
(25) Perdew, J. P.; Burke, K.; Ernzerhof, M. *Phys. Rev. Lett.* **1996**, *77*, 3865.
(26) (a) Wang, H. F.; Liu, Z. P. *J. Am. Chem. Soc.* **2008**, *130*, 10996. (b) Shang, C.; Liu, Z. P. *J. Chem. Theory Comput.* **2010**, *6*, 1136.
(27) (a) Anisimov, V. I.; Zaanen, J.; Andersen, O. K. *Phys. Rev. B* **1991**, *44*, 943. (b) Anisimov, V. I.; Solovyev, I. V.; Korotin, M. A.; Czyżyk, M. T.; Sawatzky, G. A. *Phys. Rev. B* **1993**, *48*, 16929.
(28) (a) Zhao, Y.; Truhlar, D. G. *J. Chem. Phys.* **2006**, *125*, 194101. (b) Zhao, Y.; Truhlar, D. G. *J. Chem. Phys.* **2009**, *130*, 074103. (c) Zhao, Y.; Truhlar, D. G. *Theor. Chem. Acc.* **2008**, *120*, 215. (d) Zhao, Y.; Truhlar, D. G. *J. Phys. Chem. A* **2006**, *110*, 13126.
(29) Adamo, C.; Barone, V. *J. Chem. Phys.* **1999**, *110*, 6158.
(30) (a) Labat, F.; Baranek, P.; Domain, C.; Minot, C.; Adamo, C. *J. Chem. Phys.* **2007**, *126*, 154703. (b) Labat, F.; Baranek, P.; Adamo, C. *J. Chem. Theory Comput.* **2008**, *4*, 341.
(31) Camellone, M. F.; Fabris, S. *J. Am. Chem. Soc.* **2009**, *131*, 10473.

ample, the calculated H_2O adsorption energies (without ZPE correction) on (101) and (001) are −0.84 and −2.97 eV, respectively, from SIESTA and −0.76 and −2.92 eV, respectively, from plane-wave methods. For total density of states (DOS) comparison of the anatase (101) and (001) surfaces, the much finer (4×4×1) *k*-point mesh was used.

To derive the free energy reaction profile, we first obtain the reaction energy of each elementary step (strictly, ΔF at 0 K, 0 bar), which is directly available from DFT total energy (ΔE) after ZPE correction. For surface reactions, ΔF at 0 K, 0 bar is a good approximation to the Gibbs free energy (G), as the temperature (T) and pressure (p) contributions are small. However, for reactions involving gaseous or liquid molecules, such as oxygen, hydrogen, and water, the large entropy term at elevated temperatures is essential in computing G. We therefore utilize standard thermodynamic data[32a] to obtain the T and p contributions to the G values of aqueous H_2O and gaseous H_2, which are 0.57 and 0.31 eV lower compared to the total energy of the corresponding free molecule (E, 0 K).[32b] The G of O_2 is derived as $G[O_2] = 4.92\ \text{eV} + 2G[H_2O] - 2G[H_2]$ according to the OER equilibrium at the standard conditions.

Finally, we need to derive the Gibbs free energy change (ΔG) of an elementary step involving protons and holes, as described by formula (1). Since electron−hole pair generation always occurs simultaneously in photocatalytic processes, it is more convenient to rewrite formula (1) as formula (2).

$$HA + h^+ \rightarrow A + H^+ \tag{1}$$

$$HA + h^+ + e^- \rightarrow A + H^+ + e^- \tag{2}$$

Using the standard hydrogen electrode (SHE) as the reference, $H^+ + e^- \rightarrow {}^1/_2\,H_2$ (pH = 0, p = 1 bar, T = 298.15 K), we get

$$\Delta G_H = \frac{1}{2}G[H_2] - G[H^+ + e^-] = 0 \tag{3}$$

Therefore, for the reaction in formula (2), the free energy change is written as

$$\begin{aligned} \Delta G &= G[A] + G[H^+ + e^-] - G[HA] - G[h^+ + e^-] \\ &= G[A] + \frac{1}{2}G[H_2] - G[HA] - |e|U \end{aligned} \tag{4}$$

where U is the electropotential of a hole (at the maximum of the valence band) with respect to SHE ($U = 0$, $\Delta G_H = 0$), and thus $|e|U$ represents the energy required to generate the electron−hole pair.[33−35]

2.2. Implementation of Parallel Periodic Continuum Solvation Model. The detailed algorithm of this method has been addressed in a series of papers by Fattebert and Gygi,[36−38] and we have implemented it previously for the calculations of solvation energies of free molecules and for periodic systems.[39] In solving the Poisson−Boltzmann equation numerically, we utilized a sixth-order finite-difference scheme that is appropriate to discretize partial differential equations with periodic boundary conditions.[40] Other details of our implementation are given in the Supporting Information. The continuum solvation model allows band structure alignment between different surfaces with the same solution level (i.e., potential zero defined at the middle of the slab in a vacuum, where the dielectric function approaches 78.36), and more importantly, it corrects the DFT energy for the long-range electrostatic interaction due to solvation.

3. Results

3.1. Surface Phases and Electronic Structure for TiO_2 Surfaces in Contact with H_2O. In photocatalytic water splitting, TiO_2 is immersed in an aqueous surrounding. It is thus essential to know the surface phase for each TiO_2 surface in contact with water. We have considered explicitly the adsorption of both molecular H_2O and dissociated H_2O (OH and H) on (101), (001), and (102) surfaces at different coverages, and the aqueous surroundings are taken into account implicitly by the continuum solvation model (unless otherwise explicitly mentioned, the continuum solvation model was always applied to describe long-range electrostatic solvation effects in this work). To measure the free energy change of the adsorption process, the quasi-differential Gibbs free energy ($\Delta G_{\text{diff}|\Delta\theta}$) is utilized, which is the free energy change per addition of $\Delta\theta$ monolayer (ML) of H_2O, defined by the equation $\Delta G_{\text{diff}|\Delta\theta} = G(\text{sur}+\Delta\theta H_2O)_{aq} - G(\text{sur})_{aq} - \Delta\theta G(H_2O)_{aq}$, where the subscript aq denotes the aqueous surrounding. A negative ΔG_{diff} (<0) means that the adsorption of H_2O is thermodynamically favored. Since H_2O adsorption involves generally the exposed cationic Ti sites, we defined the coverage of H_2O with respect to the exposed five-coordinated Ti (Ti_{5c}) on the surfaces.

We found that the (101) terrace has a poor affinity toward H_2O, as the $\Delta G_{\text{diff}|1/6\ \text{ML}}$ of molecularly adsorbed water on (101) (Figure 1b) is +0.04 eV at 1/6 ML. The dissociation of H_2O on the (101) surface is also not favored, with $\Delta G_{\text{diff}} = +0.05$ eV. Consistent with this, Diebold et al., using scanning tunneling microscopy, have shown that water adsorbs on the (101) surface only molecularly under ultra-high-vacuum conditions, and the coverage is very low (∼0.005 ML) at room temperature.[41] By contrast, on the (001) surface H_2O can dissociatively adsorb up to 1/2 ML ($\Delta G_{\text{diff}|1/4\ \text{ML}} = -0.76$, −0.58, and +0.66 eV for 1/4, 1/2, and 1 ML coverage, respectively). The dissociation leads to two upright OH's at the two neighboring Ti_{5c} sites, linked to each other via H-bonding (Figure 1c).[42,43] One of the OH's evolves from the hydrogenation of a lattice-bridging O between two Ti_{5c}'s. The (001) facet of (102) has water affinity similar to that of the (001) surface, on which H_2O can dissociatively adsorb up to 1/8 ML ($\Delta G_{\text{diff}|1/8\ \text{ML}} = -0.86$ and +0.49 eV for 1/8 and 1/4 ML coverage, respectively). On the basis of these results, we chose clean (101), 1/2 ML H_2O-covered (001), and 1/8 ML H_2O-covered (102) as the model surfaces for our investigation of OER activity.

With and without water surroundings, the redox ability of the surfaces might be quite different. It is therefore important to gather an overview of the electronic structure of (101) and (001) surfaces in aqueous solution. In Figure 2, we have plotted the total density of states (DOS) of (101), (001), and 1/2 ML H_2O-covered (001) in aqueous surroundings. We aligned the DOSs by utilizing the potential energy level in solution (∼ −4.6

(32) (a) *CRC Handbook of Chemistry and Physics*, 84th ed.; Lide, D. R., Ed.; CRC Press: Boca Raton, FL, 2003−2004. (b) Liu, Z. P.; Jenkins, S. J.; King, D. A. *J. Am. Chem. Soc.* **2004**, *126*, 10746.
(33) Valdés, Á.; Qu, Z.-W.; Kroes, G.-J.; Rossmeisl, J.; Nørskov, J. K. *J. Phys. Chem. C* **2008**, *112*, 9872.
(34) Rossmeisl, J.; Qu, Z.-W.; Zhu, H.; Kroes, G.-J.; Nørskov, J. K. *J. Electroanal. Chem.* **2007**, *607*, 83.
(35) Anderson, A. B.; Albu, T. V. *Electrochem. Commun.* **1999**, *1*, 203.
(36) Fattebert, J. L.; Gygi, F. *J. Comput. Chem.* **2002**, *23*, 662.
(37) Fattebert, J. L.; Gygi, F. *Int. J. Quantum Chem.* **2003**, *93*, 139.
(38) Fattebert, J. L.; Gygi, F. *Phys. Rev. B* **2006**, *73*, 115124.
(39) Wang, H. F.; Liu, Z.-P. *J. Phys. Chem. C* **2009**, *113*, 17502.
(40) Fornberg, B.; Sloan, D. M. *Acta Numer.* **1994**, *3*, 203.
(41) He, Y.; Tilocca, A.; Dulub, O.; Selloni, A.; Diebold, U. *Nat. Mater.* **2009**, *8*, 585.
(42) Gong, X. Q.; Selloni, A. *J. Phys. Chem. B* **2005**, *109*, 19560.
(43) Vittadini, A.; Selloni, A.; Rotzinger, F. P.; Gratzel, M. *Phys. Rev. Lett.* **1998**, *81*, 2954.

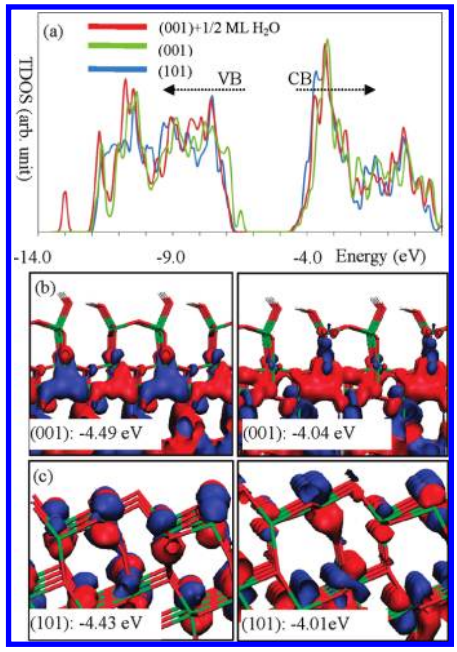

Figure 2. (a) Total density of states of three surfaces in aqueous surroundings (via continuum solvation). (b,c) 3D isosurface contour plots of selected lowest unoccupied wave functions on (001) with 1/2 ML H_2O (b) and on (101) (c) (eigenvalues are indicated). The isosurface value is set as ± 0.02 e/Å^3.

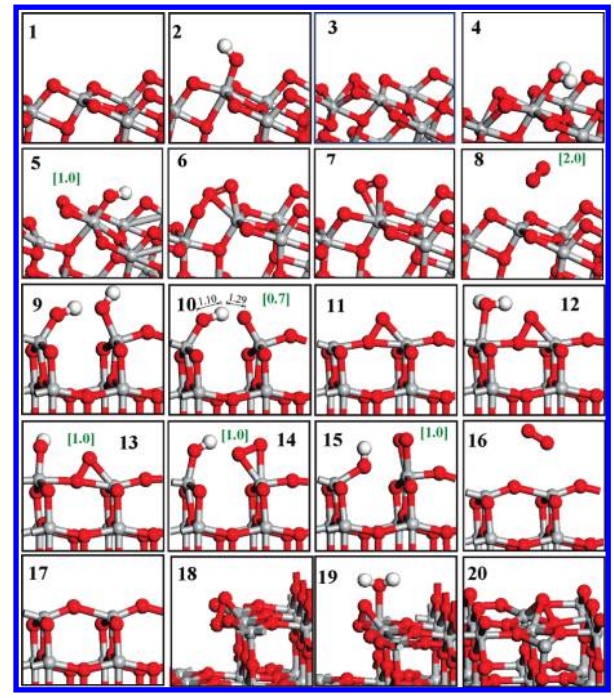

Figure 3. Optimized structures of the intermediate states in OER: **1**−**8**, anatase (101); **9**−**17**, anatase (001); **18** and **19**, rutile (100); **20**, rutile (110). The data in square brackets indicate the state with net magnetic moments (μ_B). Ti, gray; O, red; H, white.

eV is equivalent to 0 V vs SHE[44]). In terms of the valence band (VB), although the clean (001) surface has a significant larger population at the top levels of VB than does the clean (101) surface, 1/2 ML dissociated H_2O almost completely quenches this feature. This is understandable as the VB originates mainly from the O 2p states and the dissociated H_2O significantly stabilizes the surface, which shifts the O 2p statesdownward. Consistent with the large H_2O adsorption energies on (001), the DOS plot also indicates that the anatase (001) surface can be strongly stabilized in aqueous solution. This agrees with the experimental observation that the proportion of (001) in anatase crystal can be maximized in solution.[45−49]

By taking a close look at the conduction band (CB) of the DOSs, we noticed that the bottom levels of CBs on (101) have a larger population than those on (001) surfaces. To comprehend further the differences in CB, we plotted in Figure 2b,c the lowest unoccupied wave functions (LUWFs) of (101) and 1/2 ML H_2O-covered (001), whose eigenvalues are below −4.0 eV. (Only two representative LUWFs are shown for each surface; the others are available in the Supporting Information, Figure S1). Importantly, we found that the spatial distributions of LUWFs are indeed distinct between the two surfaces. The LUWFs on (001) mainly locate in the sublayers, while the LUWFs of (101) always have a significant distribution on the surface layer, as can be seen in Figure 2b,c. As the bottom of the CB is where photoelectrons stay and the surface photoelectrons are essential for reduction reaction, (101) facets are thus predicted to have a higher efficiency in photoreduction reactions. On the other hand, for oxidation reactions such as the OER, we did not find an obvious difference between the two studied anatase surfaces at the maximum VB. Further study on the kinetics of OER pathways is thus essential and will be presented in the next subsection.

The different redox behavior of surfaces manifested by the electronic structures can be used to rationalize the recent experiment by Ohno et al.,[20] who utilized scanning electron microscopy to observe the deposition sites of photo-oxidation and photoreduction products on TiO_2. Using H_2PtCl_6 as an electron scavenger, Pt was found to mainly grow on anatase (101) ($H_2PtCl_6 + 4e^- \rightarrow Pt\downarrow + 2HCl + 4Cl^-$). From our results, it is not surprising that the majority (101) surface is the site for reduction due to the accumulation of photoelectrons on the surface layer, despite the presence of OH groups on the (001) surface.

3.2. OER Mechanism on Three TiO_2 Surfaces. To map out the whole OER reaction network on the surfaces, we took a recursive trial-and-error approach, in which we investigated each "likely" oxidation channel by adding H_2O onto the surface and then removing H (proton/electron pair) stepwise until O_2 species was produced. By "likely" we mean that the reaction route must have relatively low free energy barriers, typically below 0.7 eV (the magnitude being regarded as being surmountable for reactions occurring at room temperature[26a]) at a given overpotential. In the following, we elaborate the calculated lowest energy pathways for OER on the surfaces.

The structures of the optimized key reaction intermediates are illustrated in Figure 3, numbered sequentially from **1** to **17**. The free energy profiles are shown in Figure 4, and the data are listed in Table 1, where an overpotential of 0.7 V (i.e., $U =$ 1.93 V vs SHE) is applied to deduce the reaction free energies as addressed in eq 4. The 0.7 V overpotential is theoretically

(44) Reiss, H.; Heller, A. *J. Phys. Chem.* **1985**, *89*, 4207.
(45) Han, X. G.; Kuang, Q.; Jin, M. S.; Xie, Z. X.; Zheng, L. S. *J. Am. Chem. Soc.* **2009**, *131*, 3152.
(46) Amano, F.; Prieto-Mahaney, O.-O.; Terada, Y.; Yasumoto, T.; Shibayama, T.; Ohtani, B. *Chem. Mater.* **2009**, *21*, 2601.
(47) Zhang, D. Q.; Li, G. S.; Yang, X. F.; Yu, J. C. *Chem. Commun.* **2009**, 4381.
(48) Yang, H. G.; Sun, C. H.; Qiao, S. Z.; Zou, J.; Liu, G.; Smith, S. C.; Cheng, H. M.; Lu, G. Q. *Nature* **2008**, *453*, 638.
(49) Yang, H. G.; Liu, G.; Qiao, S. Z.; Sun, C. H.; Jin, Y. G.; Smith, S. C.; Zou, J.; Cheng, H. M.; Lu, G. Q. *J. Am. Chem. Soc.* **2009**, *131*, 4078.

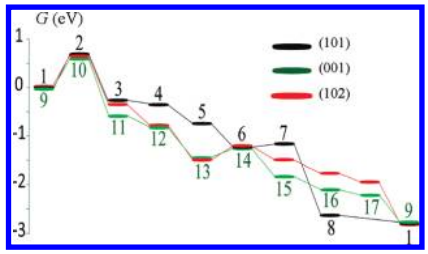

Figure 4. Free energy (G, eV) profiles of OER on (101) (black), (001) (green), and (102) (red) surfaces at an overpotential of 0.7 V (1.93 V vs SHE).

the low limit for OER to occur on all three surfaces. Considering that the minimum CB of TiO_2 is about 0.2 eV higher in energy relative to SHE, it implies that visible light above 2.1 eV (0.2 + 1.93 eV, ~590 nm) is *kinetically* enough to drive the photocatalytic OER. In reality, only ultraviolet light can drive OER on TiO_2, which is to a large extent due to the large band gap, ~3.2 eV.[10,50]

On (101) surface, the OER proceeds by the direct splitting of H_2O on a Ti_{5c} site (H_2O + **1** + h^+ → **2** + H^+) to produce an adsorbed OH (state **2**, Figure 3) since H_2O adsorption on (101) is unfavorable thermodynamically. The OH then loses a further proton, and the remaining O adatom (O_{ad}) can spontaneously lean down to bond with an adjacent lattice O (bridging O_{2c}), yielding a surface-bridging O−O (state **3**). State **3** is spin-unpolarized, implying that the bridging O−O is a peroxo-like species. At this state, the release of O_2 from the lattice is energetically highly unfavorable because reduced anatase with an oxygen vacancy is very unstable. Next, a second H_2O molecule adsorbs at the surface Ti_{5c} near the O−O species (H_2O + **3** → **4**). After the adsorbed H_2O decomposes to an adsorbed OH by losing a proton, the bridging O−O species breaks one of its Ti−O bonds, turning into a terminal O_2 (**4** + h^+ → **5** + H^+). At state **5**, the terminal O_2 species is spin-polarized (1.0 μ_B), indicating that the O−O species has become superoxo-like. Upon further losing a proton from the OH, the terminal O can lean down to connect with surface O−O (state **6**). Finally, O_2 desorbs from the surface via transition state **7** (**6** → **7**) with a very low reaction barrier (0.1 eV).

Figure 4 shows that the first proton release is kinetically important for oxygen evolution on the (101) surface: removal of the first proton in the dissociation of H_2O (**1** → **2**) must overcome 0.69 eV, even at an overpotential of 0.7 V. By closely examining the structure of state **2**, we found that the surface Ti is pulled up markedly from the surface, and the new Ti−O bond of the surface Ti−OH species is quite short, 1.80 Å. This indicates that the OH adsorbs well on the TiO_2 surface, which is consistent with the conclusion that the OH is not a radical species (spin-unpolarized), as indicated by our calculations.

As for the OER on the minority surfaces, (001) and (102), we mainly focused on the (001) facet, where the sites are partially covered by OH's. We found that the pathways and the energetics are similar for OER on the (001) surface and on the (001) facet of the (102) surface, and thus in the following only the pathway on the (001) surface is addressed, as being representative. On the (001) surface, the OER starts by deprotonation of the 1/2 ML H_2O-covered (001) surface. Similar to the case on the (101) surface, the first proton release here (**9** + h^+ → **10** + H^+) is also energetically highly unfavorable, requiring 0.61 eV at the overpotential of 0.7 V, about 0.08 eV lower compared to that on the (101) surface. Surprisingly, at state **10** the H is rather short distances from both O's (1.10 and 1.29 Å), and the [O−H−O] complex is spin-polarized (0.7 μ_B) with the spin magnetic moments localized on the two O's (0.4 and 0.3 μ_B).

Table 1. Calculated Free Energies of Elementary Steps in OER on Three Antatase Surfaces[a]

elementary step	ΔE (eV)	ΔH(0→298 K) (eV)	ΔZPE (eV)	$-T\Delta S$ (eV)	$-\|e\|U$ (eV)	ΔG (eV)
			(101)			
1 + H_2O + h^+ → **2** + H^+	2.23	−0.06	−0.02	0.47	−1.93	0.69
2 + h^+ → **3** + H^+	1.25	0.04	−0.12	−0.20	−1.93	−0.96
3 + H_2O → **4**	−0.80	−0.10	0.14	0.67	0	−0.09
4 + h^+ → **5** + H^+	1.92	0.04	−0.22	−0.20	−1.93	−0.39
5 + h^+ → **6** + H^+	1.79	0.04	−0.21	−0.20	−1.93	−0.51
6 → **7**	0.10	0	0	0	0	0.10
7 → **8**	−1.48	0	0	0	0	−1.48
8 → **1** + O_2	0.44	0.10	−0.07	−0.63	0	−0.16
			(001)			
9 + h^+ → **10** + H^+	2.91	0.04	−0.21	−0.20	−1.93	0.61
10 + h^+ → **11** + H^+	1.03	0.04	−0.14	−0.20	−1.93	−1.20
11 + H_2O → **12**	−0.98	−0.10	0.17	0.67	0	−0.24
12 + h^+ → **13** + H^+	1.81	0.04	−0.36	−0.20	−1.93	−0.64
13 → **14**	0.21	0	0	0	0	0.21
14→**15**	−0.59	0	0	0	0	−0.59
15 + h^+ → **16** + H^+	1.86	0.04	−0.03	−0.20	−1.93	−0.26
16 → **17** + O_2	0.48	0.10	−0.06	−0.63	0	−0.11
17 + H_2O → **9**	−1.30	−0.10	0.15	0.67	0	−0.58
			(102)			
9 + h^+ → **10** + H^+	2.93	0.04	−0.21	−0.20	−1.93	0.63
10 + h^+ → **11** + H^+	1.25	0.04	−0.14	−0.20	−1.93	−0.98
11 + H_2O → **12**	−1.18	−0.10	0.17	0.67	0	−0.44
12 + h^+ → **13** + H^+	1.76	0.04	−0.36	−0.20	−1.93	−0.69
13 → **14**	0.27	0	0	0	0	0.27
14 → **15**	−0.29	0	0	0	0	−0.29
15 + h^+ → **16** + H^+	1.84	0.04	−0.03	−0.20	−1.93	−0.28
16 → **17** + O_2	0.42	0.10	−0.06	−0.63	0	−0.17
17 + H_2O → **9**	−1.58	−0.10	0.15	0.67	0	−0.86

[a] The structures for the states labeled from **1** to **17** are shown in Figure 3. ΔH(0→298 K) is from ref 32a.

After the second proton removal (**10** + $h^+ \rightarrow$ **11** + H^+), a surface O−O (also a peroxo-like species) is produced, as the O adatom tends to bond with the adjacent lattice O_{2c}. The O−O forms a new linkage between two surface Ti's. Next, the second water adsorbs on one Ti neighboring the O−O (state **12**). Afterward, the adsorbed H_2O decays to an adsorbed OH by losing a proton (**12** + $h^+ \rightarrow$ **13** + H^+). At state **13**, the surface O−O species is spin-polarized (1.0 μ_B), indicating that the bridging O−O species has become superoxo-like. The bridging O−O can then shift to one Ti side, forming a terminal O_2, and at the same time the OH sinks into the bridge site between two Ti's. The structural change from state **13** to **15** has a quite flat potential energy surface, as the intermediate state **14** is only 0.21 eV less stable than state **13**. By further losing a proton from the OH, the terminal O_2 can finally desorb from the surface. The 1/2 ML H_2O-covered (001) surface is regenerated by the dissociation of H_2O.

3.3. Vibrational Frequency Analysis of Surface O−O Species. With the vibrational frequencies calculated for all the states in the OER pathway, it is worthwhile for us to examine whether the identified surface O−O intermediates are superoxo or peroxo. This also allows us to compare our mechanism with that proposed by Nakamura and Nakato,[18] who observed new IR absorption bands in rutile particles under UV irradiation by *in situ* FT-IR experiments. Two bands at 812 and 838 cm^{-1} were assigned to the O−O stretching mode of Ti−O−O−Ti and Ti−OOH^+ (appearing at low pH conditions) intermediates, respectively.

Before examining the frequency of surface species, we have first chosen to look at the reported TiO_3 and TiO_5 molecules, for which experimental data are available,[51] to validate our theoretical approach for calculating the O−O stretching frequency (ν_{O-O}). We found that the DFT calculated frequencies are generally close to the corresponding experimental values, and there is a good linear relationship between the calculated frequencies and the experimental data ($R^2 = 0.99$). (The results are listed in the Supporting Information, Table S1.) From DFT calculations, the stretching frequency of peroxo O_2^{2-} in TiO_x molecules is 890 cm^{-1} (31 cm^{-1} larger than the experimental value in (η^2-O_2)TiO), and that of superoxo O_2^- is ∼1100 cm^{-1}.

Our calculated ν_{O-O} values for the surface O−O species in the OER pathway are listed in Table 2. They are from states **3** and **4** in (101) and **11**−**15** in (001). Since experimental data for ν_{O-O} in the OER are available only on rutile crystal, we also calculated the relevant O−O states on rutile (100) (**18** and **19**, see Figure 3) and rutile (110) (**20**, see Figure 3). States **18** and **20** mimic **11**, with surface O−O only (O adatom on lattice O), while state **19** mimics **12**, having surface O−O with nearby H_2O coadsorption.

We found that, except for anatase (101), where the ν_{O-O} appears around 900 cm^{-1}, anatase (001), rutile (100), and rutile (110) can all exhibit ν_{O-O} around 850 cm^{-1}. Specifically, the ν_{O-O} values of states **12** (845 cm^{-1}), **19** (854 cm^{-1}), and **20** (832 cm^{-1}) agree generally with the experimental peroxo band at 813 cm^{-1}, considering that our calculated ν_{O-O} in (η^2-O_2)TiO molecule is 31 cm^{-1} larger than the experimental value. By further protonating the O−O species in states **12**, **19**, and **20**, we also calculated the ν_{O-O} values of the protonated O−O species to be 856, 860, and 839 cm^{-1}, respectively. These values are also close to the 838 cm^{-1} identified by experiment for the protonated peroxo species (OOH^+) species. On the basis of the good agreement with experimental frequencies, we therefore suggest that the formation of peroxo species may well be a general feature for photocatalytic water splitting on oxide surfaces, not limited to rutile TiO_2.

Table 2. Calculated O−O Stretching Frequency in the O−O Intermediate States of the OER Pathway[a]

surface	state	ν_{O-O} (cm^{-1})	d_{O-O} (Å)
anatase (001)	**11**	893	1.45
	12	845	1.49
	[**12** + H]$^+$	856	1.49
	13	1101	1.36
	14	1123	1.34
	15	1127	1.34
antase (101)	**3**	904	1.46
	4	900	1.46
rutile (100)	**18**	872	1.48
	19	854	1.48
	[**19** + H]$^+$	860	1.49
rutile (110)	**20**	832	1.48
	[**20** + H]$^+$	839	1.49

[a] [**X** + H]$^+$ represents the state **X** being protonated, forming surface OOH^+ species.

Knowing the charge state of O−O species, we were interested to find that the formal oxidation state of Ti is largely conserved as Ti^{4+} at the states involving O−O species. In the states with bare O−O species, the O−O coadsorbed with H_2O, or the protonated O−O on anatase and rutile surfaces (800−900 cm^{-1}), we can assign the O−O species to be O_2^{2-}, and thus, accordingly, all Ti are Ti^{4+}. For the O−O species in the presence of adsorbed OH, such as statea **13**−**15**, ν_{O-O} increases to ∼1100 cm^{-1} and the states are spin-polarized (1.0 μ_B), indicating the presence of a superoxo (O_2^-) together with a OH^-. Consequently, all Ti cations are still Ti^{4+}.

4. General Discussion on the Physical Origin of the High Overpotential

By comparing the OER pathways on (101), (001), and (102) as summarized in Figure 4, we can see that the first proton removal is generally the most important step for oxygen evolution on the surfaces. Considering that the (101) surface is the majority surface and the free energy change for the first proton removal in (101) is only 0.08 eV higher than that in the minority (001) surface, our results suggest that OER activity is not sensitive to the local surface structure of anatase. Therefore, it turns out to be critical to ask why the first proton removal is generally difficult and whether this can be facilitated by modifying the material, such as changing the crystal morphology (e.g., rutile, anatase) or doping with other elements.

To answer these questions, we first compared the electronic structure of the majority surfaces of rutile and anatase, since it was shown experimentally that the rutile phase is responsible for OER activity in TiO_2 powders with mixed rutile and anatase phases.[19] In Figure 5, we compare the total DOS of rutile (110) surface and anatase (101) surface in aqueous surroundings (in plotting Figure 5, we utilized 10 layers of rutile (110) to get converged DOS at the maximum of VB). As shown, the maximum of VB in rutile (110) exhibits a small shoulder peak, as indicated by the arrow in Figure 5a, which is higher in energy compared to that of anatase (101). On both rutile (110) and

(50) Gai, Y. Q.; Li, J. B.; Li, S. S.; Xia, J. B.; Wei, S. H. *Phys. Rev. Lett.* **2009**, *102*, 036402.
(51) Gong, Y.; Zhou, M. F. *J. Phys. Chem. A* **2008**, *112*, 9758.

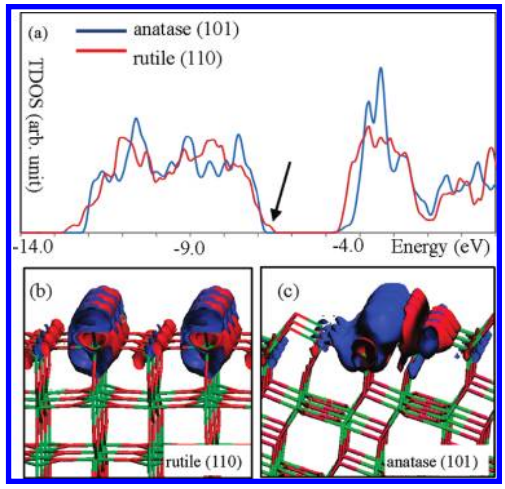

Figure 5. (a) Total density of states of rutile (110) and anatase (101) surfaces in aqueous surroundings (via continuum solvation). (b,c) 3D isosurface contour plots of the highest occupied wave functions (the maximum of VB) on the two surfaces. The isosurface value is set as ±0.02 e/Å^3.

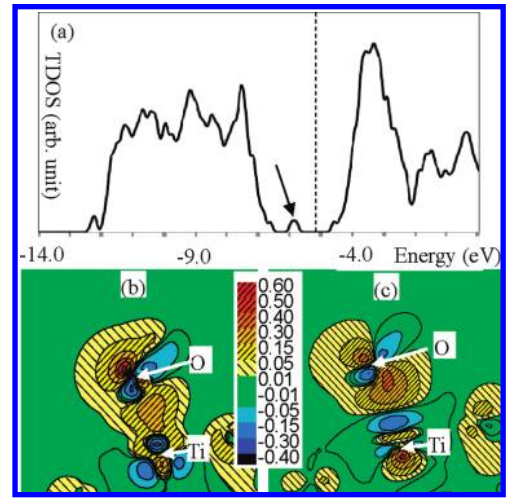

Figure 6. Total density of states of the Mo + C co-doped anatase (101) (a), and the electronic charge density difference contour plot cutting through the Ti−O(OH) bonding plane in the Mo + C co-doped anatase (101) (b) and in the pure anatase (101) (c) before and after the OH adsorption in aqueous surroundings (via continuum solvation). Positive/negative values mean electron density accumulation/depletion. The arrow in (a) indicates the introduced dopant levels.

anatase (101) surfaces, the wavefunction at the maximum of VB in anatase (101) is mainly concentrated on the two-fold lattice O's at the surface layer (Figure 5b,c). This is an indication that the photogenerated hole is accessible to both surfaces. Since the maximum of VB differs in energy for the two surfaces, it is expected that the OER activity will be different. To confirm this, we then examined the first proton removal step on the rutile (110) surface, which is similar to **1** → **2** on anatase (101). Our calculated ΔG is 0.29 eV at an overpotential of 0.7 V, which is indeed lower than that on anatase (101), consistent with the experimental finding.[19]

Naturally, one would wonder whether it is the presence of shoulder states at the maximum of VB in rutile (110) that benefits the OER. We therefore considered doping other high-valent elements in anatase to introduce the similar extra states within the gap, as shown by Gai et al.[50] For this purpose, we modeled Nb + N and Mo + C co-doped (101) and (001) slabs (concentration Ti:Nb(Mo):C(N) is 47:1:1 for (101) and 31:1:1 per slab for (001)), where the doped atoms locate at the fourth Ti layer and ninth O layer [the doped Nb(Mo) bonds directly with N(C)]. For these co-doped systems, the electrons from the donor passivate the same amount of holes on acceptor levels, and the system overall retains the intrinsic semiconducting character. Importantly, the band gap of the co-doped system is much reduced compared to that of pure anatase. As a representative, the total DOS of the Mo+C co-doped sytem is shown in Figure 6, where extra occupied states emerge above the VB of bare anatase, as indicated. The results are consistent with previous calculations by Gai et al.[50] The ΔG values for the first (**1** → **2**, **9** → **10**) and second (**2**→ **3**, **10** → **11**) proton removal steps on these doped or pure surfaces were then calculated and are listed in Table 3.

From Table 3, we can see the strong influence of the dopants on the catalytic ability. In all doped systems, the free energy for the first proton removal (ΔG_1) is much reduced, while the free energy for the second proton removal (ΔG_2) increases generally. Obviously, the Mo + C co-doped system has the highest activity among the systems. We found that the geometric relaxation at the initial and final states induced by the dopants is negligibly small since the dopants are deep in the subsurface

Table 3. Comparison of the Free Energies of the First (ΔG_1) and the Second (ΔG_2) Proton Removal Steps on the Co-Doped (Nb + N, Mo + C) and Pure Anatase (101) and (001) Surfaces at an Overpotential of 0.7 V[a]

	Nb + N	Mo + C	pure
	(101)		
ΔG_1 (eV)	0.48	0.08	0.69
ΔG_2 (eV)	−0.80	−0.39	−0.96
	(001)		
ΔG_1 (eV)	0.45	0.20	0.61
ΔG_2 (eV)	−1.08	−0.82	−1.20

[a] ΔG_1 corresponds to **1** → **2** on (101) and **9** → **10** on (001), and ΔG_2 corresponds to **2** → **3** on (101) and **10** → **11** on (001).

(see Supporting Information, Table S2). Geometrical factors thus cannot be the cause for the dramatic change in the reaction energetics.

To understand the enhanced activity in the co-doped systems, we analyzed the electronic structure for the OH adsorption on anatase surfaces. We found that the HOMO level of isolated OH radical in solution is about 0.4 eV lower than the VB top of TiO_2 (see Supporting Information, Figure S2), indicating electron transfer from the surface to OH upon OH adsorption. As the surface is stoichiometric before the OH adsorption, this implies that the surface becomes "over-oxidized" upon OH adsorption. Our Mulliken charge analysis confirms that the adsorbed OH is −0.3 charged for OH on anatase (101). Furthermore, the electronic charge density difference before and after OH adsorption on anatase (101) has also been calculated, and the contour plots cutting through the Ti−O(OH) bonding plane are shown in Figure 6b,c for Mo + C co-doped anatase (101) and for pure anatase (101). We can see that, in addition to the charge transfer from substrate to OH, covalent bonding between OH 2p orbitals and the Ti 3d orbtials is also present, which provides direct evidence for the critical roles of d-orbitals in photocatalytic OER. Importantly, compared to the pure anatase system, the polarization and the charge transfer from Ti to OH are more obvious in the Mo + C co-doped system, which indicates stronger Ti−OH bonding in the co-doped system.

On the basis of the analyses above, we are finally able to answer the question of how to enhance OER activity in general. In forming a bond between OH and the TiO_2 surface, the Ti−OH bonding state is below the maximum of VB of TiO_2,[52] and there is obvious net electron transfer from the TiO_2 surface to OH. However, such electron transfer is at the expense of the TiO_2 lattice bonding, since the TiO_2 surface is in stoichiometry and oxidation of the surface is energetically unfavorable. In the presence of co-dopants, extra occupied states above the VB are introduced, which can enhance the electron transfer to the adsorbed OH and thus facilitate the first proton removal step. Similarly, one can understand why the rutile phase has a higher activity than anatase. In short, the high overpotential of OER can be attributed to the instability of the surface-adsorbed OH state after the first proton removal. By introducing occupied levels above VB of pure TiO_2, the OER activity can be significantly enhanced.

By comparing our mechanism with those previously proposed in experiments, we emphasize that there are no adsorbed OOH and HOOH species in the identified OER path. This is in fact reasonable, as these hydrogenated species (OOH, HOOH) become increasingly unstable at the high overpotential condition of OER. Furthermore, the exposed coordination-unsaturated Ti's are revealed to be the major reaction sites, although the holes are trapped in the surface lattice O's. The covalent bonding identified to be achieved by the p-states of the intermediate oxidative species and the d-states is critical to facilitate the oxygen evolution. Energetically, it is unfavorable that OER is initiated by direct attack of a H_2O molecule at a surface lattice O of TiO_2, as proposed by Nakamura and Nakato.[18]

5. Conclusions

This work represents a comprehensive survey of the reaction network for OER on various anatase surfaces in aqueous surroundings by integrating first-principles slab calculations with a parallel implementation of the periodic continuum solvation model. The microscopic mechanism of the OER is identified, and the critical roles of the exposed coordination-unsaturated Ti atoms are highlighted. Consistent with experimental findings, the surface peroxo and superoxo groups are the common key intermediates. Differently structured anatase surfaces are investigated for their OER activity, which reveals that OER is not sensitive to the local surface structure of anatase but is strongly influenced by the energy position of the maximum of VB. Both the addition of dopants and the change in phase morphology may influence OER activity strongly. Our calculations suggest that visible light (<∼590 nm) is enough to drive photocatalytic OER kinetically on TiO_2 surfaces. More detailed results are summarized as follows.

(i) In aqueous solution, the minority anatase (001) surface is terminated by 0.5 ML dissociated water molecules, while the majority (101) surface is hydrophobic. From the electronic structure at the minimum of CB, the anatase (101) surface has a stronger ability to accumulate photoelectrons than the 0.5 ML H_2O-covered (001) surface. This indicates that the photocatalytic reduction process can be better catalyzed by the majority (101) surface. On the other hand, the electronic structures at the maximum of VB are very similar for the (101) and the H_2O-covered (001) surfaces.

(ii) The high overpotential of OER can be attributed to the high energy cost associated with the first proton removal step. This step requires 0.69, 0.63, and 0.61 eV at an overpotential of 0.7 V on anatase (101), (102), and (001) surfaces, respectively. After the first proton removal, an adsorbed OH state is formed, where the stoichiometric TiO_2 surface is oxidized due to the electron flow from the surface to the adsorbed OH group. The presence of d-states helps to stabilize the adsorbed OH via covalent bonding.

(iii) By co-doping with Nb + N or Mo + C, the surface OH state can be stabilized due to the extra occupied states above VB. This helps to reduce the overpotential dramatically. The same understanding can be extended to rationalize the higher activity of rutile phase than anatase phase. Our results provide general rules for the design of better photocatalysts for OER.

Acknowledgment. This work is supported by NSF of China (20825311, 20773026, 20721063), Science and Technology Commission of Shanghai Municipality (08DZ2270500), and Program for Professor of Special Appointment (Eastern Scholar) at Shanghai Institute of Higher Learning. W.G. thanks the Special Funds for Major State Basic Research Projects of China (2005CB321700) and Science and Technology Commission of Shanghai Municipality (09ZR1401900) for financial support.

Supporting Information Available: Details of the implementation of the parallel periodic continuum solvation model; experimental and calculated vibrational frequencies of TiO_3, TiO_5, and H_2O_2; geometric relaxation caused by the dopants; contour plot of LUWFs on (101) and (001); DOS of anatase (101) and isolated OH radical in aqueous solution. This material is available free of charge via the Internet at http://pubs.acs.org.

JA105340B

(52) Imanishi, A.; Okamura, T.; Ohashi, N.; Nakamura, R.; Nakato, Y. *J. Am. Chem. Soc.* **2007**, *129*, 11569.